© 2017. Published by The Company of Biologists Ltd | Development (2017) 144, 4091-4102 doi:10.1242/dev.153114

STEM CELLS AND REGENERATION

RESEARCH ARTICLE

# Interorgan regulation of *Drosophila* intestinal stem cell proliferation by a hybrid organ boundary zone

**Jessica K. Sawyer[1,2], Erez Cohen[2,3] and Donald T. Fox[1,2,3,*]**

## ABSTRACT

The molecular identities and regulation of cells at interorgan boundaries are often unclear, despite the increasingly appreciated role of organ boundaries in disease. Using *Drosophila* as a model, we here show that a specific population of adult midgut organ-boundary intestinal stem cells (OB-ISCs) is regulated by the neighboring hindgut, a developmentally distinct organ. This distinct OB-ISC control occurs through proximity to a specialized transition zone between the endodermal midgut and ectodermal hindgut that shares molecular signatures of both organs, which we term the hybrid zone (HZ). During homeostasis, proximity to the HZ restrains OB-ISC proliferation. However, injury to the adult HZ/hindgut drives upregulation of *unpaired-3* cytokine, which signals through a Signal transducer and activator of transcription (STAT) protein to promote cell division only in OB-ISCs. If HZ disruption is severe, hyperplastic OB-ISCs expand across the interorgan boundary. Our data suggest that interorgan signaling plays an important role in controlling OB-ISCs in homeostasis and injury repair, which is likely to be crucial in prevention of disease.

**KEY WORDS: *Drosophila*, Hindgut, Midgut, Organ boundary, Intestinal stem cell**

## INTRODUCTION

Interorgan boundaries, such as those in the intestine, provide an opportunity to understand an emerging area of stem cell research: signaling to stem cells from a neighboring tissue. Stem cells at interorgan boundaries are near cells from a functionally distinct organ. Therefore, such stem cells could reside in a very different tissue environment than other seemingly identical stem cells elsewhere in the same organ. Very little is known about stem cell control at intestinal organ boundaries, yet hyperproliferation of putative injury-activated stem cells and altered cell fate at the human esophagus/stomach boundary is linked to Barrett's esophagus, a condition that increases cancer risk (Badreddine and Wang, 2010; Hvid-Jensen et al., 2011; San Roman and Shivdasani, 2011). New understanding of the complex interorgan stem cell control at intestinal organ boundaries could be aided by development of a simple, genetically tractable model tissue.

Insect intestinal organ boundaries (Akai and King, 1982; Nation, 2001) are an excellent candidate to model interorgan stem cell control. At both the foregut/midgut and midgut/hindgut organ boundaries are cell populations classically defined as imaginal rings, which are enriched for Wnt (Wingless, Wg) ligands (Bodenstein, 1950; Fox and Spradling, 2009; Robertson, 1936; Takashima et al., 2008; Tian et al., 2016). The boundary between the endodermal midgut (small intestine) and the pylorus of the ectodermal hindgut (large intestine) demarcates a sharp contrast in intestinal cell architecture and cell turnover rates. The adult *Drosophila* midgut, which is rich in microvilli (Fig. 1A′), turns over weekly under rich diet conditions. The adult midgut is composed of multipotent intestinal stem cells (ISCs) and their progeny, the secretory enteroendocrine cells (EEs) and enteroblasts (EBs), which differentiate into polyploid absorptive enterocytes (ECs) (Apidianakis et al., 2009; Buchon et al., 2009a,b; Guo and Ohlstein, 2015; Micchelli and Perrimon, 2006; Ohlstein and Spradling, 2006, 2007; Zeng and Hou, 2015). This proliferative organ responds to tissue loss via compensatory stem cell proliferation (Apidianakis et al., 2009; Buchon et al., 2009a,b; Chatterjee and Ip, 2009; Jiang et al., 2009). Adjacent to the posterior midgut is the pyloric sphincter of the *Drosophila* hindgut (Fig. 1A, red), the functional analog of the mammalian ileocecal sphincter, which lacks microvilli but is chitin rich (Fig. 1A′). Under normal homeostatic conditions, the pylorus is a quiescent diploid tissue as it has negligible levels of cell cycle activity (Fox and Spradling, 2009). Following injury, the pylorus does re-enter the cell cycle, but instead of cell division it undergoes compensatory cellular hypertrophy and wound-induced endocycles, which replicate the DNA without cell division, generating polyploid pyloric cells (Losick et al., 2013). We previously proposed that injury-responsive stem cells were in the Wnt-positive imaginal ring region (hereafter referred to as Wg ring), but it remained possible that these cells were in the posterior midgut adjacent to the Wg ring (Fox and Spradling, 2009). The distinct cell types of the midgut/hindgut boundary and their potential role in the homeostasis/tissue repair program of each organ remained to be determined.

Here, we characterize the cellular architecture and function of the *Drosophila* midgut/hindgut boundary. In doing so, we show that the adult Wg imaginal ring is a transition zone that shows hybrid (both midgut and hindgut) gene expression. The function of this hybrid zone (HZ) is to repress proliferation of organ-boundary intestinal stem cells (OB-ISCs) located in the midgut, which reside immediately adjacent to the anterior boundary of the HZ. Relative to most other posterior midgut ISCs, OB-ISCs exhibit low cell cycle rates and are resistant to *Notch*-mediated stem cell tumor formation. When injury locally disrupts the hybrid zone, OB-ISC cell division is induced. Under conditions of severe injury, hyperplastic OB-ISCs often cross the midgut/hindgut boundary through disrupted segments of the HZ. OB-ISC division is regulated by release of the JAK-STAT ligand Unpaired-3 (Upd3) from the hindgut and HZ. HZ-derived Upd3 is both necessary and sufficient for organ nonautonomous control of OB-ISC proliferation. Our results

[1]Department of Pharmacology & Cancer Biology, Duke University Medical Center, DUMC Box 3813, Durham, NC 27710, USA. [2]Regeneration Next, Duke University Medical Center, DUMC Box 3813, Durham, NC 27710, USA. [3]Department of Cell Biology, Duke University Medical Center, DUMC Box 3813, Durham, NC 27710, USA.

*Author for correspondence (don.fox@duke.edu)

D.T.F., 0000-0002-0436-179X

**Received 5 April 2017; Accepted 15 September 2017**

Development (2017) 144, 4091-4102 doi:10.1242/dev.153114

identify a HZ as a strategy for regulating signaling between adjacent organs. We also find that interactions between organs at a boundary can profoundly influence stem cell activity. Thus, use of a HZ between different organs can preserve organ integrity and maintain cell fate between two distinct, yet adjacent, organs.

## RESULTS

### The Wg ring is a dynamic HZ adjacent to midgut ISCs/EBs

We previously identified putative stem cell activity at the injured adult *Drosophila* midgut/hindgut boundary (Fox and Spradling, 2009). Given the complexity of cell types in this region, we next

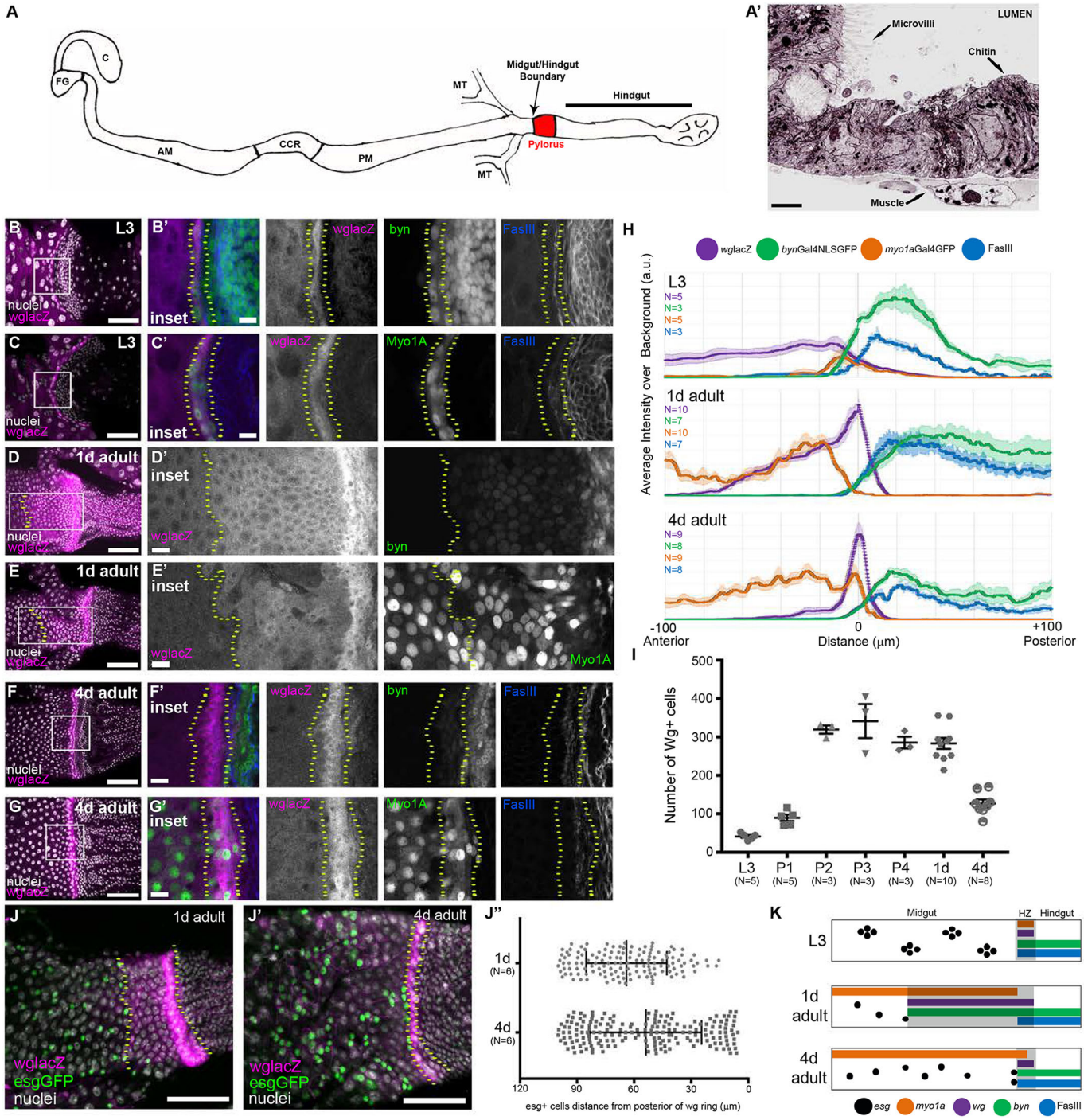


**Fig. 1. The Wg ring is a dynamic HZ adjacent to midgut ISCs/EBs.** (A) Schematic of the *Drosophila* intestine. AM, anterior midgut; C, crop; CCR, copper cell region; FG, foregut; MT, malpighian tubules; PM, posterior midgut. (A′) Electron micrograph illustrating the phenotypic differences at the midgut/hindgut boundary. There is a clear transition from cells with microvilli to cells that lack microvilli, but are chitin rich. (B-I) The HZ is present throughout development: L3 (B-C′), 1 day adult (D-E′), 4 days adult (F-G′). (H) Line profiles of midgut, HZ and hindgut markers. Data represent mean±s.e.m. (I) The number of *wg*+ cells over time, L3 to adulthood. Data represent mean±s.e.m. (J-J″) *esg*+ cells stay at the anterior edge of the *wg* expression domain. Data represent mean±s.e.m. of all *esg*+ cells from six animals. Unpaired, two-tailed *t*-test, $P$=0.0006. (K) Model of the HZ during development. Genotypes and markers are indicated within panels; yellow dotted lines indicate the HZ. Scale bars: 2 μm in A′; 10 μm in B′,C′,D′,E′,F′ and G′; 50 μm in B,C,D,E,F,G,J and J′.

Development (2017) 144, 4091-4102 doi:10.1242/dev.153114

characterized each epithelial population in the midgut/hindgut boundary at single-cell resolution. A ring of epithelial cells that strongly expresses *wg* (the Wg ring) resides directly at the midgut/hindgut boundary (Fox and Spradling, 2009; Takashima et al., 2008; Takashima and Murakami, 2001; Tian et al., 2016). To determine whether the cells in the Wg ring possess molecular characteristics of hindgut or midgut, we used a *lacZ* trap of the *wg* gene (*wglacZ*) to mark this population and then examined two well-known markers of both the midgut and hindgut. First, we examined animals during late third instar larval development (L3). The Wg ring during L3 consists of ∼40 cells that also express two hindgut markers: the pan-hindgut transcription factor *brachyenteron* (*byn*) and the cell adhesion molecule Fasciclin III (FasIII, or Fas3) (Fig. 1B,B′,H,I). Anterior to the Wg ring, we did not detect the expression of *byn* and FasIII is weakly accumulated. Additionally, the same *byn*+FasIII+ cells of the L3 Wg ring cells also express *Myosin 31DF* (*Myo1a*), a marker of midgut differentiated enterocytes, as previously reported (González-Morales et al., 2015) (Fig. 1C,C′,H,I). We further found that a second midgut enterocyte marker, Nubbin (or POU domain protein 1, Pdm1), co-localizes with *Myo1a* in the L3 Wg ring (Fig. S1A-A″). Together, these results suggest that just prior to metamorphosis, cells of the Wg ring simultaneously express not only multiple hindgut markers but also well-established markers of midgut enterocytes.

During metamorphosis, much of the intestinal epithelium undergoes histolysis and is reformed, while the region around the Wg ring remains intact (Fox and Spradling, 2009; Robertson, 1936; Takashima et al., 2008). We next examined how cell fate and number in the Wg ring are altered during metamorphosis. At two distinct stages of pupal development, *wg* and *byn* expression in the Wg ring remain tightly correlated (Fig. S1C-C‴,E-E‴). We also find *Myo1a* expression in some *wg*+*byn*+ cells (Fig. S1D-D‴,F-F‴). During pupation, the Wg ring continues to express markers of both the midgut and hindgut and increases ∼sevenfold in cell number (Fig. 1I). As adulthood begins (1 day), the Wg domain can be subdivided into two regions. In the anterior region, low level *wg*+ cells express *byn* and *Myo1a*, and low levels of FasIII (Fig. 1D-E′, H). Closer to the hindgut, these same markers are present, but *wg*, FasIII and *byn* are higher, while *Myo1a* is lower (Fig. 1D-E′). In mature adults (4 days, after gut remodeling), the Wg domain shrinks to ∼125 cells (Fig. 1F-G′,H,I). We propose that this results from expression changes, as we did not see evidence of cell death in early adulthood (Fig. S1G-G″; see Fig. 4B,B′ for positive control). As the Wg domain recedes, adult midgut ISCs and their immediate EB daughters, marked by the transcription factor *escargot* (*esg*), appear next to the midgut/hindgut boundary (Fig. 1J-J″). This finding is consistent with previous reports that ISCs may migrate to the posterior midgut (Takashima et al., 2016, 2013), and suggests that the extent of the Wg domain determines the posterior position of midgut ISCs/EBs.

Our data from larval and pupal stages suggested that many *wg*+ cells might be uncommitted to a particular organ identity during development. We next investigated whether the mature adult Wg ring retains a mixed organ identity or acquires a specific organ fate. Indeed, the adult Wg ring continues to co-express *byn*, FasIII, *Myo1a* and Pdm1, and retains hybrid organ characteristics (Fig. 1F-G′,H; Fig. S1B-B‴). Thus, the Wg domain is dynamic in size from late larva (L3) to mature adult. Further, at all stages examined, the Wg ring domain contains cells that express markers of both the midgut and hindgut (Fig. 1K). Owing to the persistent dual-organ gene expression in this midgut/hindgut transition zone, we term this region the HZ.

### The larval HZ significantly contributes to the formation of the adult posterior midgut and anterior hindgut

Previous studies suggested that during metamorphosis, the epithelial region containing the adult HZ and a portion of the posterior midgut arises from *byn*+*FasIII*+ cells in the larval hindgut pylorus that transdifferentiate into *byn*–, *FasIII*–, *Myo1A*+, *Pdm1*+ enterocytes (Fig. 2A) (Takashima et al., 2008; Takashima et al., 2013). However, these studies used population-wide lineage tracing approaches, which have the caveat that they cannot distinguish subpopulations of cells expressing a given promoter (Fox et al., 2008). Additionally, our finding that a hybrid midgut/hindgut

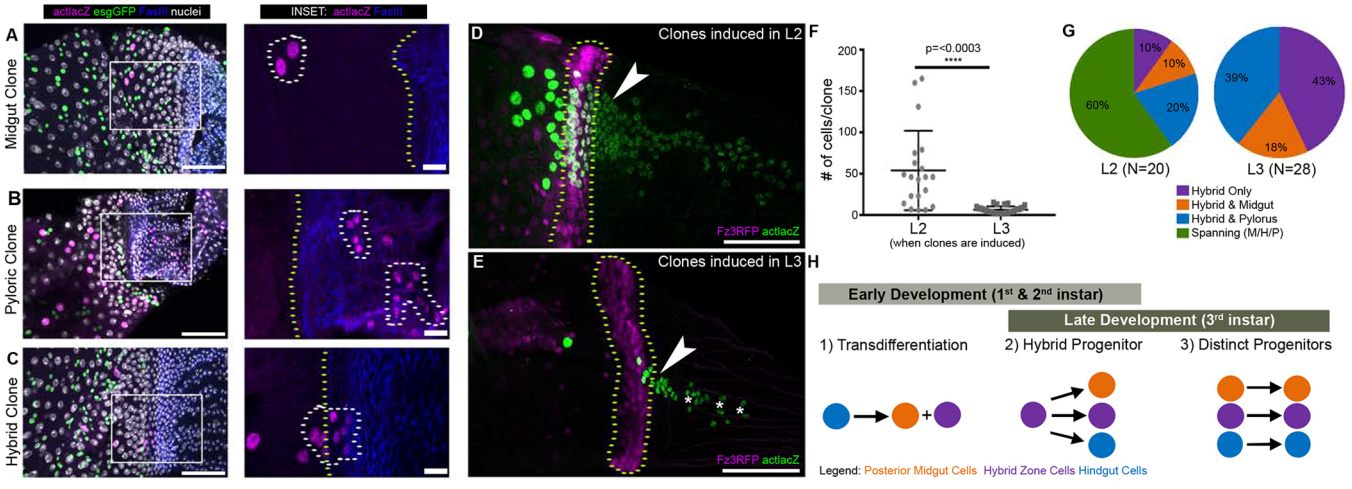


**Fig. 2. The larval HZ significantly contributes to the adult posterior midgut and anterior hindgut.** (A-C) Examples of clone types observed: midgut (A), pyloric (B), hybrid (C); *esg*GFP marks midgut ISCs/EBs. Scale bars: 50 µm (10 µm in insets). (D) Example of a clone induced in L2 (second instar); *esg* was not labeled in this experiment. Scale bar: 50 µm. (E) Example of a clone induced in L3 (third instar); *esg* was not labeled in this experiment. Scale bar: 50 µm. (F) Clones induced earlier in development that overlap the HZ are larger. Data represent mean±s.e.m. Unpaired, two-tailed *t*-test, unequal variance. (G) Clones that span the posterior midgut, HZ and pylorus are only observed when clones are induced early in development. Chi-Square Fisher's Exact test, $P \leq 0.0001$. (H) Models illustrating potential origins of the HZ. Genotypes and markers are indicated within panels; yellow dotted lines indicate the HZ, white dotted lines indicate clones, arrowheads indicate hybrid clones, asterisks indicate pyloric clones.

Development (2017) 144, 4091-4102 doi:10.1242/dev.153114

population persists throughout metamorphosis (Fig. S1C,E) suggests that the HZ and adjacent posterior midgut might instead arise from either a hybrid progenitor, or from distinct progenitor pools, rather than from transdifferentiation of pyloric cells (Takashima et al., 2013). Therefore, we followed the lineage of individually labeled cells (see Materials and Methods) during larval and pupal development. In addition to providing unbiased, random labeling, we observed little to no background labeling with this system (Fig. S2A-B′). This low background labeling enabled us to avoid confusing our labeling with noninduced labeling at unspecified times in development/adulthood.

We first induced clones just prior to metamorphosis (L3; see Materials and Methods). Our lineage results from 316 independent clones did not reveal any evidence of continuous clones that encompass the pylorus, HZ and adjacent posterior midgut. Rather, based on clone location and size, we observed three distinct epithelial clonal patterns in the region from the posterior midgut to the adult hindgut pylorus (Fig. 2A-C). The first pattern we observed consisted of clones not in the HZ, but in the nearby posterior midgut (55% of all clones, average size 2.9±0.1) (Fig. 2A; Fig. S2C,D). The vast majority (98%) of these clones consisted only of polyploid midgut enterocytes. A small subset of these midgut clones (2%) contained ISCs/EBs (*esg*+). We never observed overlap between *esg*+ clones and the HZ, suggesting that *esg*+ ISCs/EBs do not generate the majority of the posteriormost midgut region or the adult HZ, in agreement with previous findings (Takashima et al., 2013). The second class of clones that we observed resided entirely within the pylorus (hindgut) and not in the HZ (38% of all clones, average size 6.2±0.3) (Fig. 2B; Fig. S2C,D). Finally, we observed a unique class of HZ-localized clones (7% of all clones, average size 10.6±0.9) (Fig. 2C; Fig. S2C,D).

HZ clones were distinct from midgut and pyloric clones in multiple ways. In addition to being significantly larger than midgut or pyloric clones (Fig. S2D), only this class of clones overlaps the HZ/hindgut boundary as defined by FasIII (Fig. 2C; Fig. S2E). Typically, HZ clones have two more cells posterior to the FasIII boundary than anterior (six cells posterior versus four cells anterior) (Fig. S2E). To further clarify the patterns of clones that overlap the HZ, we co-imaged with a marker of the HZ. HZ clones occasionally overlapped with the posterior midgut (typically extending one cell diameter into the posterior midgut; 18% of HZ clones) (Fig. 2G). We more frequently observed HZ clones that were entirely contained in the HZ (43% of HZ clones) (Fig. 2G) or HZ clones that overlapped the anterior pylorus (extending up to six cell diameters into the anterior pylorus; 39% of clones) (Fig. 2E,G). Further, none of the HZ clones (0/20) contain *esg*+ ISCs/EBs. This finding reinforces the model that the HZ does not arise from these *esg*+ midgut cells, and also shows that *esg*+ and HZ cells have distinct developmental origins. Taken together, these clonal data rule out the idea that a common hindgut progenitor generates the entire adult pylorus, HZ and adjacent posterior midgut during metamorphosis.

It remained possible that posteriormost midgut, HZ and pyloric adult populations share a common progenitor earlier in development. We thus induced clones during earlier larval development (L1/L2). Indeed, clones recovered from these early induction time points were larger and encompassed the midgut, HZ and pylorus (Fig. 2D versus E,F,G). Given our clonal data and the expansive nature of the HZ during metamorphosis (Fig. S1), we propose that a hybrid progenitor acts early in larval development to produce the posteriormost region of the adult midgut, the adult HZ and the adult pylorus (Fig. 2H). By the onset of metamorphosis, these three cell populations appear more distinct, with hybrid only and hybrid/pyloric clones becoming more prominent when induced later in development (Fig. 2G; Fig. S2F). This contrasts with the model that these cell populations are formed by transdifferentiation of larval hindgut cells (Takashima et al., 2013).

### Midgut stem cells adjacent to the adult HZ are less proliferative and resist tumor formation

Given the unique gene expression and lineage of the adult HZ and its juxtaposition to developmentally distinct ISC/EBs in the neighboring midgut, we next examined whether the HZ microenvironment might influence adjacent midgut cell cycle activity. A recent study (Tian et al., 2016) used *wg* pathway mutants to interrogate the function of *wg* signaling in the developing midgut. They found that *wg* signaling is important for fate establishment and proliferation control near the midgut/hindgut boundary. However, it remained unclear whether this phenotype resulted from disrupting development or adult homeostasis. Further, given our identification of distinct cell types, including the HZ at the midgut/hindgut boundary, the role of each cell population at this boundary was also unclear. We thus investigated whether interorgan (HZ/hindgut to midgut) regulation of midgut ISCs occurs specifically during adult homeostasis and injury repair, and identified which specific cell types are involved.

We first examined homeostasis. A previous report found *frizzled-3* (*fz3*), a downstream effector of the Wg pathway, to be expressed in the vicinity of Wg boundaries and in some adult ISCs/EBs, including the most posterior midgut region (R5/P4) (Tian et al., 2016). Using an *fz3* reporter, we find that a subpopulation of the R5/P4 midgut region ISC/EB cells (~20%) are *esg*+*fz3*+ (Fig. 3A-A″). These *fz3*+ midgut ISC/EB cells are primarily found within 30 µm of the HZ (Fig. 3B). We next closely examined cell cycle dynamics in this 30 µm region relative to other midgut cells that were considered to be in the same region (R5/P4) (Buchon et al., 2013; Marianes and Spradling, 2013). Our results show that this region consists of two cell populations with distinctly different cell cycle rates. By feeding mature adults the thymidine analog bromodeoxyuridine (BrdU) to mark S-phase activity, we noticed a significant reduction in *esg*+ ISC/EB cell cycling within 30 µm of the midgut/hindgut boundary, as defined by FasIII (average number of *esg*+, BrdU+ cells: 0-30 µm=2.5±1.2 versus 70-100 µm=12.3±2.6; total *esg*+ cells: 0-30 µm=6.0±2.2 versus 70-100 µm=16.2±3.2) (Fig. 3C-C″,D). We also noted this reduction when examining all BrdU-labeled midgut cells, which includes the endocycling enterocytes (average number of BrdU+ cells: 0-30 µm=7.5±2.7 versus 70-100 µm=24±3.8) (Fig. S3A).

We also asked if the reduced cell cycle rates observed in the 30 µm midgut region adjacent to the HZ impact tumor development. Previous studies in the midgut revealed that loss of *Notch* in ISCs leads to the formation of stem cell tumor-like hyperplasia (Guo and Ohlstein, 2015; Micchelli and Perrimon, 2006; Ohlstein and Spradling, 2006, 2007). We examined the posterior midgut adjacent to the HZ in animals expressing *Notch* RNAi specifically in *esg*+ ISCs and associated EBs. As a proxy for tumor formation, we counted clusters of *esg*+ ISC/EBs (see Materials and Methods). Several days after *Notch* RNAi expression, within 70-100 µm of the HZ, we frequently observed tumors with >six *esg*+ cells (22%) (see Materials and Methods). However, within 0-30 µm we rarely observed these larger tumors (~6%) (Fig. 3E-G; Fig. S3C-E′), which mirrored the reduction in cell cycle rates we observed in this region (Fig. 3C-D). Indeed, as the distance from the HZ increases,

Development (2017) 144, 4091-4102 doi:10.1242/dev.153114

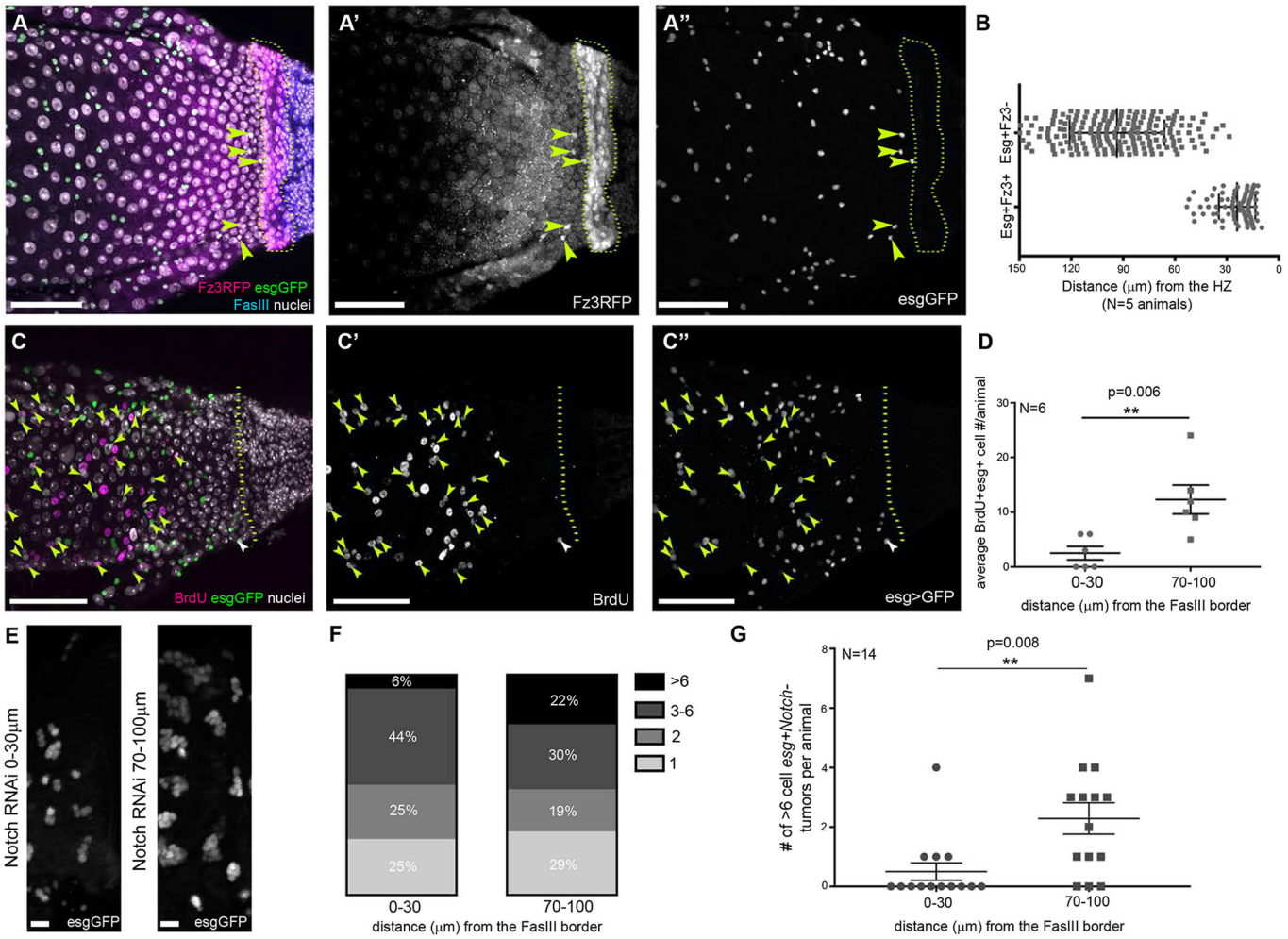


**Fig. 3. Midgut stem cells adjacent to the adult HZ are less proliferative and resist tumor formation.** (A-A″) *esg*+ cells near the HZ are *fz3*+; yellow arrowheads indicate *esg+fz3+* cells. (B) *esg+fz3+* are mostly within 30 µm of the HZ. Data represent mean±s.e.m. of all *esg+fz3+* cells from six animals. Unpaired, two-tailed *t*-test, unequal variance, $P \leq 0.0001$. (C-C″) Near the HZ fewer cells cycle; yellow arrowheads indicate *esg*+BrdU+ cells beyond 30 µm from the HZ, white arrowhead indicates an *esg*+BrdU+ cell within 30 µm of the HZ. (D) Significantly fewer *esg*+ cells are BrdU+ 0-30 µm from the HZ compared to 70-100 µm from the HZ. Paired, two-tailed *t*-test. (E) *Notch* RNAi stem cell tumors are smaller near the HZ. (F,G) *Notch* RNAi stem cell tumors of >six cells are found less frequently 0-30 µm from the HZ compared to 70-100 µm from the HZ. (F) Percentages of *esg*+ tumor sizes in *Notch* mutant animals 0-30 µm from the HZ compared to 70-100 µm from the HZ. Chi-Square Fisher's Exact test, $P=0.002$. (G) In *Notch* mutant animals, more *esg*+ tumors of >six cells are found 0-30 µm from the HZ compared to 70-100 µm from the HZ. Data represent mean±s.e.m. Paired, two-tailed *t*-test. Genotypes and markers are indicated within panels; yellow dotted lines indicate the HZ. Scale bars: 50 µm in A-A″,C-C″; 10 µm in E.

we noted an increase in the size of the tumors after loss of *Notch* in ISCs (Fig. S3B,D-E′). To confirm that this difference in *Notch* tumor formation was not caused by the lack of *Notch* ligand, we examined the localization of Delta (Dl) in the midgut, and readily detected Dl+*esg*+ ISCs/EBs throughout the posteriormost region of the midgut (Fig. S3F). In summary, during adult homeostasis, we find a unique ISC/EB cell population that lies adjacent to the HZ. Relative to neighboring midgut ISCs, which were previously considered as part of the same cell population, this population exhibits cell cycle rates that are much lower than their neighbors, are *fz3*+, and are resistant to stem cell tumor formation after loss of Notch signaling. We define these cells as organ-boundary intestinal stem cells (OB-ISCs).

### Injury to the adult HZ/hindgut drives OB-ISCs into the cell cycle

We next examined how the HZ and neighboring OB-ISCs respond to injury in adults. We previously used a transient injury system to injure the adult pylorus (see Materials and Methods) and identified putative stem cell activity either in or near the Wg ring (Fox and Spradling, 2009). Having now characterized at single-cell resolution the architecture and developmental origin of this region, we injured the adult HZ and hindgut and examined whether stem cell division is part of the response to injury at this organ boundary. To do this, we transiently expressed the pro-apoptotic genes *head involution defective* (*hid*) and *reaper* (*rpr*) specifically in adults (see Materials and Methods). Cell death, monitored by Death caspase-1 (Dcp-1) accumulation, was only induced in the HZ and pylorus (Fig. 4A-C). Cell cycle re-entry after injury, as monitored by BrdU, is specific to the region surrounding the HZ (Fig. S4C versus D). As previously reported, cells in the pylorus either die or re-enter the endocycle to repair damage via cellular hypertrophy (Fig. 4D-E′) (Losick et al., 2013). Cells in the HZ also undergo cell death, as evidenced by Dcp-1 and TUNEL staining (Fig. 4A-B′; Fig. S4A-B′), whereas HZ cells that do not undergo cell death re-enter the cell cycle (Fig. 4E).

Development (2017) 144, 4091-4102 doi:10.1242/dev.153114

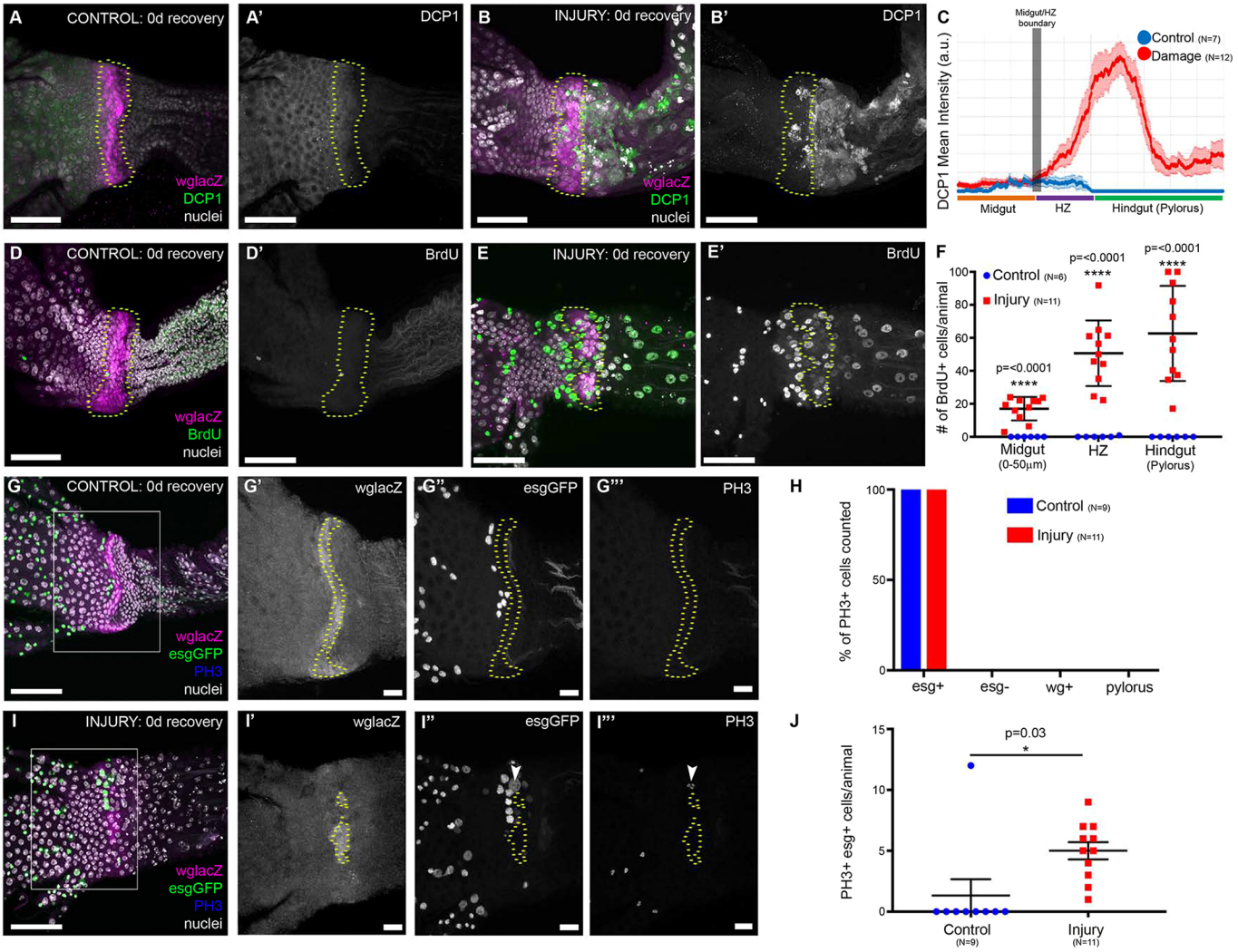


**Fig. 4. Injury to the adult HZ/hindgut drives OB-ISCs into the cell cycle.** (A-B′) Injury is specific to the HZ/hindgut. Dcp-1 is not observed in the absence of injury (A,A′). After injury, via *byn*Gal4-driven apoptosis, DCP1 is seen in the HZ/hindgut, but not the midgut (B,B′). (C) Relative DCP1 levels in control versus injury. Data represent mean±s.e.m. (D-F) Injury induces cell cycle re-entry. Few cells cycle in the absence of injury (D,D′), while many cells re-enter the cell cycle after injury, even in the midgut (E,E′). (F) Quantification of BrdU+ cells in the posteriormost midgut, HZ and the hindgut. Data represent mean±s.e.m. Multiple *t*-tests, false discovery determined using the two-stage linear step-up procedure of Benjamini, Krieger and Yekutieli (2006) with Q=1%. (G-J) Injury to the HZ promotes *esg*+ mitosis. *esg*+PH3+ cells are rarely observed in the absence of injury (G-G‴), but are frequently observed after injury (I-I‴). (H) Only *esg*+ cells are PH3+ with or without injury. Data represent the % of PH3+ cells that were also *esg*+, *esg*−, *wg*+ or FasIII+ (pyloric). (J) More cells in the posterior midgut are *esg*+PH3+ after injury. Data represent mean±s.e.m. Unpaired, two-tailed *t*-test, unequal variance. Genotypes and markers are indicated within panels; yellow dotted lines indicate the HZ. Scale bars: 50 µm in A-E′,G and I; 10 µm in G′-G‴ and I′-I‴.

Although cell cycle re-entry was expected in *byn*+ cells, what was unexpected was our observation that *byn*− cells in the adjacent midgut also re-enter the cell cycle, despite not being injured (Fig. 4E-F; Fig. S4A-B′). We previously found a localized population of putative injury-responsive stem cells that is positive for the mitotic marker phospho-histone H3 (PH3), but it remained unclear whether these cells were in the Wg ring or HZ. To clarify this, we examined PH3 along with markers for the HZ (*wg*) and OB-ISCs and associated EBs (*esg*). Strikingly, we never observed PH3+ HZ or pyloric cells, either with or without injury (Fig. 4G-I‴). These data show that the adult hindgut and associated HZ do not retain any proliferative capacity, but instead these cells undergo injury-induced endocycles (Losick et al., 2013). Furthermore, we find that all hindgut injury-induced PH3+ cells are *esg*+. After injury, *esg*+ cells are more frequently PH3+ (Fig. 4J). We also examined Dl expression after injury, and found an increased incidence of Dl+*esg*+ cells at the midgut/hindgut border after injury, indicating that PH3+ OB-ISCs likely divide to expand after injury (Fig. S3F-G″). These results show that after injury to the HZ and pylorus in adult animals, the pylorus and the HZ undergo the endocycle, but do not proliferate, and *esg*+ cells (likely the OB-ISCs) proliferate.

### Injury to the adult HZ/hindgut causes OB-ISC hyperplasia

We next determined the long-term outcome of induced midgut OB-ISC proliferation after injury to the adult HZ/hindgut. To do so, we examined the number of OB-ISCs and their daughter EBs (*esg*+) in the range of 0-30 µm and 70-100 µm from the HZ at multiple time points of recovery. We found greater numbers of *esg*+ cells close to the HZ (0-30 µm) in injured adult animals compared with controls (Fig. 5A), confirming that OB-ISCs divide to expand after injury. Strikingly, when comparing the 0-30 µm and 70-100 µm intervals

Development (2017) 144, 4091-4102 doi:10.1242/dev.153114

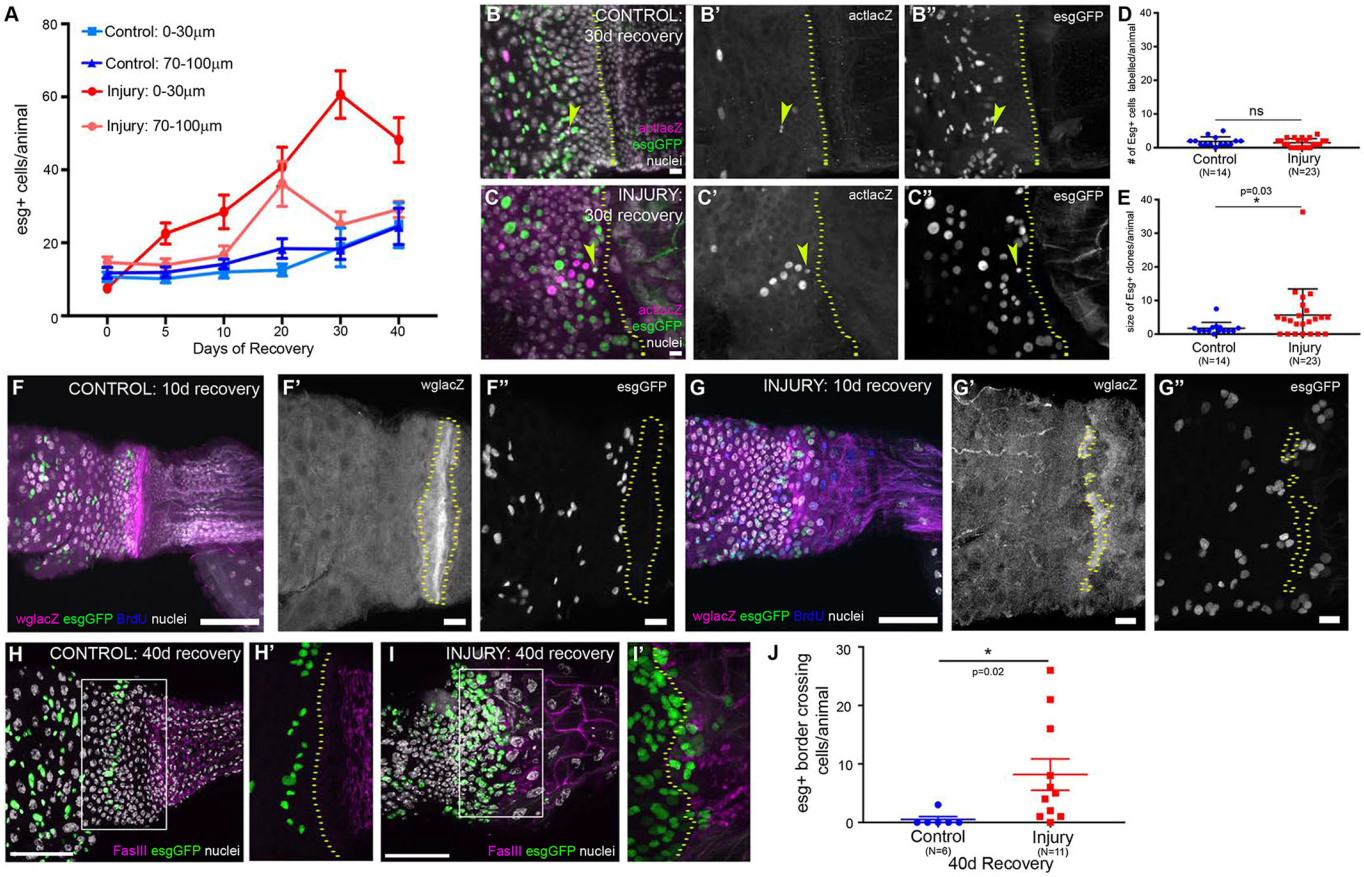


**Fig. 5. Injury to the adult HZ/hindgut causes OB-ISC hyperplasia.** (A) After injury, *esg*+ cells near the HZ expand. Data represent mean±s.e.m. (see also Fig. S5A). (B-E) This expansion is driven by *esg*+ cell division. Control (B-B″) and injury clone (C-C″) examples; arrowheads indicate a marked *esg*+ cell clone. (D) Lineage tracing marks a similar number of *esg*+ cells. Data represent mean±s.e.m. Unpaired, two-tailed *t*-test, unequal variance. (E) *esg*+ clones are larger after injury. Data represent mean±s.e.m. Unpaired, two-tailed *t*-test, unequal variance. (F-G″) Injury creates breaks in the HZ. In the absence of injury, the HZ remains intact (F-F″). After injury, breaks are frequently observed and *esg*+ are found posterior to the HZ (G-G″). (H-J) *esg*+ cells cross the FasIII boundary. *esg*+ cells rarely cross the boundary in the absence of injury (H,H′). After injury, *esg*+ cells do cross the boundary (I,I′). (J) Quantification of *esg*+ cells that cross the boundary after injury. Data represent mean±s.e.m. Unpaired, two-tailed *t*-test, unequal variance. Genotypes and markers are indicated within panels; yellow dotted lines indicate the HZ. Scale bars: 50 µm in F,G,H and I; 10 µm in B,C,F′,F″,G′ and G″.

in injured animals, we find that this expansion of *esg*+ cells is specific to the 0-30 µm range population, especially beyond 20 days after recovery (Fig. 5A). This suggested that the OB-ISC response to injury, in a neighboring organ, is a locally restricted response. Using more precise bins within a 110 µm range from the HZ, we further find that the increase in *esg*+ cells originates very close to the HZ, and gradually expands in an anterior direction (Fig. S5A).

We next considered two possibilities for the expansion of OB-ISCs near the injured HZ. The first possibility was that this expansion represents symmetric ISC division, potentially reflecting an inability of OB-ISCs to differentiate (Antonello et al., 2015; Chen et al., 2016; Meng and Biteau, 2015; O'Brien et al., 2011; Zhai et al., 2015). The second possibility was that OB-ISCs both increase in number and generate new enterocytes, perhaps in response to the loss of the HZ after injury (symmetric and asymmetric divisions). We distinguished between these possibilities by combining FLP-mediated lineage tracing and Gal4-mediated genetic cell ablation injury systems (each described earlier) in an *esg-GFP* animal. A similar number of *esg*+ cells are labeled per animal in both control and injury conditions (1.9±0.4 versus 1.4±0.3) (Fig. 5D). However, *esg*+ clones are larger in injured animals, supporting the idea that OB-ISCs divide more frequently after injury (1.7±0.5 versus 5.7±1.6) (Fig. 5B-C″,E). *esg*– cells are labeled at the same frequency in control and injured animals (7.6±1.2 versus 5.2±1.0) (Fig. S5B) but clones are also of a similar small size (nearly always one cell, occasionally two cells), as expected, given that ISCs are the source of the vast majority of cell division in the midgut, with or without injury (1.6±0.2 versus 1.1±0.1) (Fig. S5C). Of the multicellular *esg*+ cell-containing clones, almost all clones examined also contained *esg*– cells, supporting the model that injury promotes both symmetric and asymmetric divisions of OB-ISCs (Fig. S5D). This might reflect an interorgan tissue repair response (see Discussion).

A likely role of an organ boundary is to prevent mixing of cells from distinct organs. To examine this possibility, we tracked *wglacZ* expression following injury to the adult HZ/hindgut and recovery to observe the morphology of the HZ. In animals in which injury was more severe, at 10 days of recovery, we find frequent breaks in the Wg region (average breaks per animal, two; average length of break, 12 µm) (Fig. 5F-G″; Fig. S5E,F). Given that we observe gaps in the HZ, we next examined whether the excess OB-ISCs entered the hindgut through these gaps. We find that *esg*+ cells often invade breaks in the HZ 10 days after injury (Fig. 5F″ versus G″). Indeed, more breaks in the HZ lead to more OB-ISCs invading through and

Development (2017) 144, 4091-4102 doi:10.1242/dev.153114

around the HZ (Fig. S5G). Forty days after injury we find many OB-ISCs cells that have crossed into the hindgut (Fig. 5H-J). Taken together, our data demonstrate that injury to the adult HZ stimulates OB-ISC division. Under severe injury conditions, the HZ is disrupted, which allows OB-ISCs to invade across the organ boundary. Our results underscore the role of the adult HZ in repressing division and maintaining organ identity on both sides of the organ boundary.

### OB-ISCs respond to injury-induced JAK-STAT signaling

Given the gradual increase in OB-ISC proliferation next to the injured adult HZ, we next searched for molecular mechanisms driving this hyperplasia. The JAK-STAT ligand *upd3* (IL-6-like) is known to promote the proliferation of ISCs after enterocyte loss (Biteau et al., 2008; Jiang et al., 2009). We find that *upd3* is robustly expressed in the HZ and pylorus after injury (Fig. 6A,A′ versus B,B′). Next, we used *wg*Gal4 to express ectopic *upd3* specifically in the adult HZ and find that this is sufficient to drive neighboring midgut cells to re-enter the cycle, as measured by BrdU incorporation (Fig. 6C-E). This response is highly specific to the midgut. BrdU+ pyloric cells are occasionally observed after *upd3* overexpression (OE), but are only found within 5-10 µm of the HZ, while BrdU+ midgut cells are frequently found ∼100 µm from the HZ (Fig. 6D, BrdU+ pyloric cells: control=0.4±0.4, upd3OE=6.4 ±2.4). This suggests that HZ-derived *upd3* activity preferentially impacts the OB-ISCs, possibly reflecting polarized JAK-STAT signaling (Sotillos et al., 2008). Next, to test whether pylorus-derived *upd3* is sufficient to drive pyloric cells into S-phase, we drove ectopic *upd3* expression in the adult hindgut, using *byn*Gal4. Unlike HZ-specific *upd3* expression, in *byn*-induced *upd3*-expressing animals we observe a robust pyloric cell cycle re-entry response (Fig. S6A versus B). To confirm that ectopic *upd3* promotes a similar cell cycle response (i.e. mitosis) as seen in OB-ISCs after injury, we examined the mitosis marker PH3 and found that ectopic *upd3* expression from the HZ is sufficient to increase proliferation adjacent to the HZ (Fig. S6C-E). Given that we previously found that only ISCs divide with or without injury (Fig. 4H), we conclude that *upd3* expression is sufficient to promote the proliferation of OB-ISCs.

Next, we tested whether JAK-STAT signaling is necessary for the cell cycle response at the injured midgut-hindgut boundary. We thus generated animals that were homozygous for a temperature-sensitive allelic combination of *Stat92E*, in combination with our injury scheme (see Materials and Methods) (Decotto and Spradling, 2005). When animals were shifted to the restrictive temperature to simultaneously injure animals while inactivating *Stat92E*, we found a significant decrease in the number of BrdU+ cells in injured *Stat92E* animals (Fig. 6F-K). Interestingly, this decrease was more pronounced in the posterior midgut than in the HZ/pylorus (∼12-fold versus ∼2-fold decrease; Fig. 6J versus K). This mirrors our results with UAS-*upd3* driven from the HZ, and reinforces the idea that JAK-STAT signaling is required for an organ nonautonomous injury response in the posterior midgut.

In parallel, we tested whether lack of the Unpaired family ligands *upd2* and *upd3* could block the injury response (see Materials and Methods) (Osman et al., 2012). In both *upd3* single mutant and *upd2,3* double mutant hemizygous animals, we observed a similar decrease in cell cycle response at the injured midgut-hindgut boundary as for *Stat92E* animals (Fig. 6L-Q; Fig. S6F). However, this decrease was not as pronounced as *Stat92E* knockdown, suggesting that other JAK-STAT ligands might compensate when *upd2* and *upd3* are removed. Taken together, our data suggest that injury to the adult HZ both relieves the proliferation block of OB-ISCs near the HZ, and promotes proliferation of OB-ISCs by inducing JAK-STAT signaling, which is both necessary and sufficient for the OB-ISC injury response.

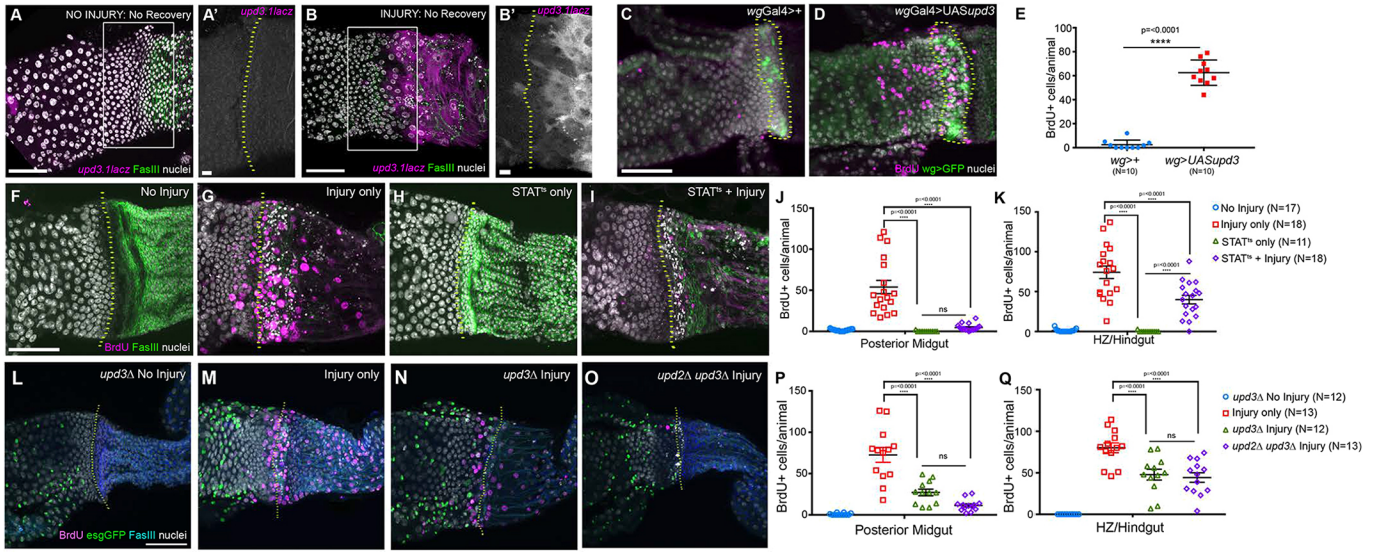


**Fig. 6. OB-ISCs respond to injury-induced Upd3.** (A-B′) *upd3* is induced after injury. *upd3* is rarely observed in the absence of injury (A,A′), but is strongly induced after injury (B,B′). (C,D) Ectopic *upd3* expression, with *wg*Gal4, drives cells in the HZ and midgut cells to re-enter the cell cycle. (E) The number of BrdU+ cells in the HZ and midgut after injury is significantly higher with *upd3* expression than without *upd3* expression. Data represent mean±s.e.m. Unpaired, two-tailed *t*-test, unequal variance. (F-K) Knockdown of *Stat92E*. (F-I) Blocking *Stat92E* function results in a reduction of injury-dependent BrdU incorporation, primarily in the posterior midgut. (J) BrdU incorporation in the posterior midgut. Data represent mean±s.e.m. (K) BrdU incorporation in the HZ/hindgut. Data represent mean±s.e.m. (L-Q) Knockdown of *upd3* and *upd2/3*. (L-O) Blocking Upd signaling results in a reduction of injury-dependent BrdU incorporation, primarily in the posterior midgut. (P) BrdU incorporation in the posterior midgut. Data represent mean±s.e.m. (Q) BrdU incorporation in the HZ/hindgut. Data represent mean±s.e.m. For J-K, P and Q, a one-way ANOVA with Tukey's multiple comparisons test was used. Genotypes and markers are indicated within panels; yellow dotted lines indicate the HZ. Scale bars: 50 µm in A,B,C,F and L; 10 µm in A′ and B′.

Development (2017) 144, 4091-4102 doi:10.1242/dev.153114

## DISCUSSION

Very little is known about control of cell fate and proliferation across boundaries of functionally distinct organs. Similarly, we have a poor understanding of how stem cells in one organ are influenced by a juxtaposed organ. Our work demonstrates that a HZ, with gene expression from both the endodermal midgut and ectodermal hindgut, acts during adult homeostasis to repress normal or tumorous (*Notch* RNAi) proliferation in nearby *fz3*+ OB-ISCs of the midgut (Fig. 7A). Injury to the adult hindgut and HZ alleviates this proliferation block, through release of *upd3* cytokine in the HZ. By examining the HZ long term after injury recovery, we observe that in cases where the HZ is significantly injured, its absence promotes invasion of hyperplastic OB-ISCs across the interorgan boundary (Fig. 7B). Collectively, our results establish the midgut/hindgut boundary as a model to understand both interorgan stem cell regulation and hyperplastic growths that invade across organ boundaries.

### The *Drosophila* adult hindgut lacks proliferative cells, even under injury conditions

Previously, we refuted the claim that the Wg ring/HZ harbored cells that were constitutively active hindgut stem cells, which had led to this region being termed the 'hindgut proliferative zone' (HPZ) (Takashima et al., 2008). Our previous work did leave open the possibility that the Wg ring cells might serve as tissue repair stem cells, only proliferating after injury (Fox and Spradling, 2009). However, the detailed marker analysis conducted in this study revealed that it is in fact the ISCs immediately adjacent to the Wg ring/HZ, termed OB-ISCs, which proliferate in response to hindgut/HZ injury in adults. Thus, it is now clear that there is no adult HPZ, even under injury conditions.

The injury responses at the midgut-hindgut boundary appear to function in tissue injury repair. As we noted previously, the injury protocol that we used here does not alter fly lifespan if the injury is acute, while chronic injury at this region drastically reduces the fly lifespan (Fox and Spradling, 2009). Further understanding the cellular nature of injury repair at the midgut/hindgut boundary will provide insight into organ boundary repair mechanisms. We speculate that asymmetric divisions of OB-ISCs contribute to repair by either producing new HZ enterocytes, as part of an interorgan stem cell repair response, or producing new midgut enterocytes to maintain tissue integrity (Fig. 7B). Our data also suggest that under severe injury conditions, HZ loss and OB-ISC hyperplasia lead to a breakdown of the organ boundary (Fig. 7B). However, it remains possible that OB-ISCs hyperplasia is beneficial after a severe injury. It is tempting to speculate that hypertrophy in the HZ/pylorus might be insufficient for repair, and the neighboring midgut contributes to repair to maintain intestinal integrity.

### Use of a HZ as a strategy to maintain two distinct organs

Our study reveals that use of a HZ is a strategy for transitioning between cell fates at an organ boundary. We postulate that the HZ has two important roles in the *Drosophila* intestine: (1) to maintain organ integrity throughout development, and (2) to mediate the transition between two distinct organs in both function and proliferative capacity. First, the HZ is a distinct landmark that likely directs the adoption of appropriate cell fates and coordinates morphogenesis of two structurally distinct organs during development. Second, the midgut is an actively proliferative adult tissue, while the hindgut is postmitotic. The pylorus, analogous to the mammalian ileocecal valve, is a contractile valve that helps to move food through the intestine. Under steady-state conditions, the HZ may suppress proliferation near this contractile sphincter tissue to keep the lumen clear of apoptotic cells and promote the flow of intestinal contents. This region of the intestinal tract is also prone to bacterial infection and scarring, highlighting its likely specialized regulation (Heimpel and Angus, 1960; Pan and Jin, 2014; Reed and Orr-Weaver, 1997). Thus, accurately defining the molecular identity of intestinal boundaries such as the midgut-hindgut boundary will increase understanding of both the development and maintenance of such boundaries.

### OB-ISCs likely reside in specialized microenvironments

In *Drosophila* and mammals, the anterior-posterior patterning of the intestine is first specified by gradients of several growth factor pathways, including Wnt, and further sharpened by Hox family homeodomain proteins and region-specific transcription factors (Nakagoshi, 2005; Zorn and Wells, 2009). In the mammalian intestine, there are both clear and imprecise morphological boundaries, but the molecular determinants of both these types of

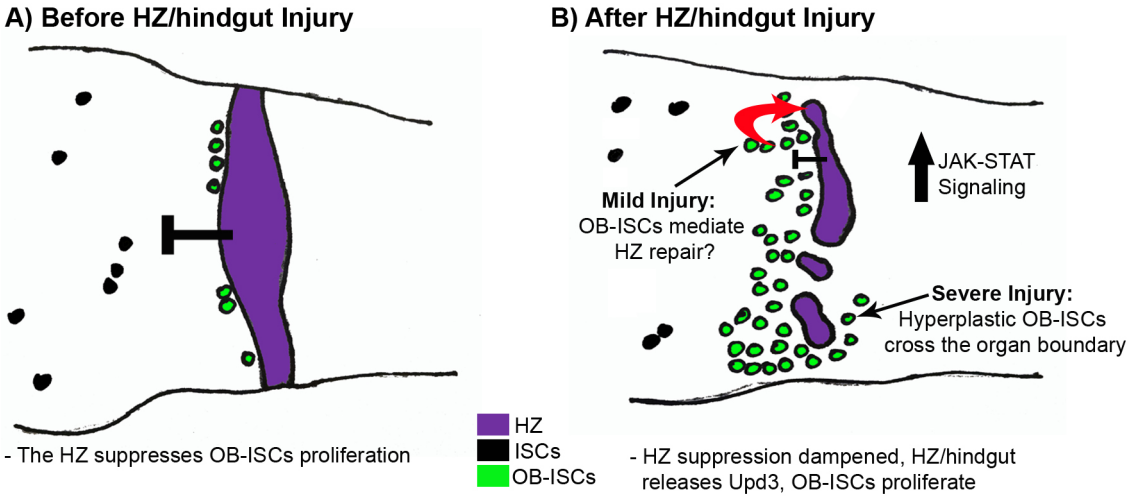


**Fig. 7. Model of OB-ISC response to injury.** (A) Before injury: OB-ISCs reside adjacent to the HZ, which suppresses proliferation relative to other R5 ISCs. (B) After injury: injury disrupts the HZ, activates JAK-STAT signaling and promotes OB-ISC proliferation. If the injury is severe, some OB-ISCs cross the organ boundary.

Development (2017) 144, 4091-4102 doi:10.1242/dev.153114

boundaries are often less clear (San Roman and Shivdasani, 2011). An example of a gastrointestinal disease that develops at an intestinal boundary is Barrett's esophagus, a metaplasia in which squamous distal esophageal cells are replaced with columnar stomach/intestine-like cells (Falk, 2002; Shaheen and Richter, 2009).

In our model, we find that after injury to the adult HZ/hindgut, OB-ISCs undergo hyperplasia and invade across an organ boundary in response to injury. This is remarkably similar to what is seen in a murine model of Barrett's esophagus, in which a small population of residual embryonic cells that resides at the squamocolumnar junction is activated upon injury and leads to their aberrant expansion across the esophagus/stomach boundary (Wang et al., 2011). This observation, along with our current work, supports the idea that stem cell displacement, and not oncogenic mutations, may be sufficient to initiate dysplasia. Importantly, dysplasias are increasingly appreciated to set the stage for cancer progression in the intestine (Flejou, 2005; Harpaz and Polydorides, 2010).

Our work further suggests that OB-ISCs are influenced by signals in their local microenvironments, and can respond to injury in a neighboring organ. Given the distance of OB-ISC injury response from HZ-derived Upd3, JAK-STAT signaling might be activated by a long-range relay mechanism, as Upd3 is not typically thought to diffuse long distances. Transcriptional profiling of the midgut has revealed that within the midgut organ, ISCs have different gene expression signatures based on their position (Dutta et al., 2015; Marianes and Spradling, 2013). From this profiling work, it is appreciated that ISCs in the most posterior portion of the midgut (R5) have a higher expression of JAK-STAT pathway genes, suggesting that these ISCs might be more poised to respond to the injury-induced *upd3* that we observe in adults (Dutta et al., 2015). Interestingly, a recent study in a murine model of Barrett's esophagus suggests that intestinal injury can increase IL-6 (the mammalian *upd3* homolog), which contributes to the progression of Barrett's and subsequent development of esophageal adenocarcinoma (Quante et al., 2012). Taken together, our data highlight the importance of interorgan boundaries as specialized stem cell microenvironments, which likely strongly influence stem behavior during both homeostasis and after injury.

In conclusion, our work provides insight into how cells residing at organ boundaries function to maintain boundary integrity during adult homeostasis and after tissue injury in adult animals. Further, our results highlight the importance of future studies of stem cells at organ boundaries as they likely reside in unique microenvironments that will differentially influence their behavior.

## MATERIALS AND METHODS

### Fly stocks

All flies were raised at 25°C on standard media (Archon Scientific) unless otherwise indicated. FlyBase (http://flybase.org) describes full genotypes for the stocks used in this study from the Bloomington Drosophila Stock Center: *wg>lacZ* (#1567), *wg>Gal4* (#48754), *act≫lacZ* (#6355), *hsFLP*$^{12}$ (#1929), *Stat92E*$^{F}$ (#24757), *Stat92E*$^{06346}$ (#11681), *upd3Δ* (#55728) and *upd2Δ,upd3Δ* (#55729). The other stocks were generous gifts: *byn>Gal4* (Singer et al., 1996), *esg>Gal4* (Bruce Edgar, University of Utah, Salt Lake City, UT, USA), *Myo1a>Gal4* (Ken Irvine, Rutgers University, NJ, USA), *upd3.1lacZ* and *UASupd3* (Huaqi Jiang, UTSW, Dallas, TX, USA), UAS*Notch*RNAi (Sara Bray, University of Cambridge, UK), *fz3*RFP (Andrea Page-McCaw, Vanderbilt University, Nashville, TN, USA), *esg*GFP (Carnegie Fly Trap, #P01986).

### *Drosophila* genetics

We dissected females for all experiments, unless otherwise noted. For developmental lineage analysis, we heat shocked (37°C water bath) *hsFLP; esgGFP; actin-FLPout-lacZ* L2 and L3 larvae once for 40 min, and aged flies until adulthood (4 days after eclosion) at 25°C to examine clones. Clones were defined as any *lacZ*+ nuclei that were adjacent to each other (thus single-labeled cells were not scored) (Fig. S2B,B′). Given that ∼68% of animals (L3 induction) and ∼92% of animals (L2 induction) contained no clones, and that the distribution of clone size was extremely uniform (Fig. 2F), we were able to conclude that the vast majority of clonal events were derived from a single progenitor. To examine *Notch* tumor-like growths, we used *esg>Gal4* to drive *UASNotch* RNAi for 10-15 days at 30°C. As a proxy for tumor growth, we counted the number of *esg*+ cells, although we acknowledge that this provides an underestimate of tumor size, as *Notch* tumors are also known to contain an excess of *esg*–, Pros+ EEs. To induce injury we aged newly eclosed flies at 18°C for 4 days, shifted to 30°C for 48 h to induce injury, shifted to 18°C for recovery, for the number of days indicated in figures (genotype: *esg*GFP/*wglacZ; byn>Gal4*, *tubGal80*$^{ts}$*, UAShid, UASrpr/+* or *TM6B/+* for controls). For overexpression of *upd3*, we aged newly eclosed flies at 18°C for 4 days, shifted to 30°C for 4 days to induce *upd3* expression with either *wg*Gal4 or *byn*Gal4. For temperature-sensitive *Stat92E* knockdown experiments, we aged newly eclosed flies at 18°C for 4 days, shifted to 30°C for 48 h to induce injury and STAT knockdown, and dissected animals immediately after injury (genotype: *UAShid, UASrpr/+; byn>Gal4*, *tubGal80*$^{ts}$*, Stat92E*$^{F}$*/Stat92E*$^{PZ06}$). For *upd* knockdown experiments, we aged newly eclosed males at 18°C for 4 days, shifted to 30°C for 48 h to induce injury and *upd* knockdown, and dissected animals immediately after injury (genotype: *upd3Δ/Y* or *upd2Δ, upd3Δ/Y; esg*GFP/+*; byn>Gal4*, *tubGal80*$^{ts}$*, UAShid, UASrpr/+*).

### Cell cycling and cell death assays

To determine cycling in WT animals, 2-day-old animals were fed 2.5 mg/ml BrdU in 5% sucrose for 5 days. For injury BrdU feedings, flies were fed 2.5 mg/ml BrdU in 5% sucrose for 24 h on day 2 of the 30°C shift. To detect mitotic cells, flies were fed 0.2 mg/ml colcemid (Sigma-Aldrich) in 5% sucrose for the last 12 h of the 2-day 30°C shift. TUNEL analysis was performed with an *in situ* cell death detection kit (Roche) as described previously (Schoenfelder et al., 2014).

### Fixed imaging

Electron microscopy was performed as described in Schoenfelder et al. (2014). For antibody staining, tissues were dissected in 1× PBS and immediately fixed in 1× PBS, 3.7% paraformaldehyde and 0.3% Triton-X for 30 min. Immunostaining was performed in 1× PBS, 0.3% Triton-X and 1% normal goat serum. The following antibodies were used in this study: anti-FasIII (DSHB, 7G10, 1:50), anti-Beta-Galactosidase (Abcam, ab9361, 1:1000), anti-Prospero (DSHB, MR1A, 1:20), anti-DCP1 (Cell Signaling, Asp261, 1:1000), anti-BrdU (Serotec, 3J9, 1:200), anti-Phospho-Histone 3 (Cell Signaling, #9706, 1:1000), anti-Delta (DSHB, C594, 1:50), anti-Pdm1 (generously shared by Steve Cohen, University of Copenhagen, Denmark, 1:10). All secondary antibodies used were conjugated with Alexa Fluor dyes (Invitrogen, 1:500). Tissues were mounted in Vectashield (Vector Laboratories). Images were acquired with the following: an upright Zeiss AxioImager M.2 with Apotome processing (10× NA 0.3 EC Plan-Neofluar air lens or 20× NA 0.5 EC Plan-Neofluar air lens), an inverted Zeiss LSM510 (10× NA 0.3 EC Plan-Neofluar air lens or 40× NA 1.3 EC Plan-Neofluar oil immersion lens), or an inverted Leica SP5 (40× NA 1.25 HCX PL APO oil immersion lens).

### Image analysis

Image analysis was performed using ImageJ (Schneider et al., 2012), including adjusting brightness/contrast, *Z* projections and cell counts. Line prolife analysis (Fig. 1) was performed as follows: for each animal, two 150 µm rectangular areas were selected, spanning the region from the center of Wg ring into the midgut (−150 to 0 µm) or the pylorus (0 to 150 µm). An additional area with no visible fluorescence was selected to calculate threshold intensity per channel per animal. Each rectangular selection was then broken up to ∼500 lines, and each line was analyzed separately for RGB intensities per pixel (0.21 µm) using a publicly available

Development (2017) 144, 4091-4102 doi:10.1242/dev.153114

RGB_Profiler ImageJ plugin (https://imagej.nih.gov/ij/plugins/rgb-profiler.html). For each animal, the analysis produced ∼350,000 individual measurements per channel per rectangle. Using R (3.3.1), the values were then averaged across the 500 lines to produce mean intensity/distance from the Wg ring. Relative fluorescence intensity was calculated by subtracting the threshold intensity per animal from the mean pixel intensity, producing a single dataset containing the relative fluorescence intensity means for each pixel per animal (∼1500 data points per animal). Finally, the relative fluorescence intensity was averaged across animals, producing a single relative fluorescence intensity per pixel across a 200 µm distance.

#### Acknowledgements

The following kindly provided reagents used in this study: Bloomington *Drosophila* Stock Center, Developmental Studies Hybridoma Bank, Ken Irvine, Sara Bray, Bruce Edgar, Huaqi Jiang, Andrea Page-McCaw and Steve Cohen. We thank Ruth Montague, Emily Bowie, Michael Sepanski and Benjamin Stormo for technical assistance; and Ken Poss, Purushothama Rao Tata, Jacob Sawyer and Fox laboratory members for valuable comments on the manuscript.

#### Competing interests

The authors declare no competing or financial interests.

#### Author contributions

Conceptualization: J.K.S., E.C., D.T.F.; Methodology: J.K.S.; Validation: J.K.S.; Investigation: J.K.S., E.C.; Data curation: J.K.S., E.C.; Writing - original draft: J.K.S., D.T.F.; Writing - review & editing: J.K.S., D.T.F.; Visualization: J.K.S., E.C.; Supervision: J.K.S., D.T.F.; Funding acquisition: J.K.S., D.T.F.

#### Funding

This work was supported by the National Institutes of Health [GM118447 and GM109538], the National Institute of General Medical Sciences [GM118447 to D.F. and GM109538 to J.S.] and Duke University [Duke Regeneration Next Initiative postdoctoral fellowship to J.S.]. Deposited in PMC for release after 12 months.

#### Supplementary information

Supplementary information available online at
http://dev.biologists.org/lookup/doi/10.1242/dev.153114.supplemental

#### References

**Akai, H. and King, R. C.** (1982). *Insect Ultrastructure*. New York: Plenum Press.
**Antonello, Z. A., Reiff, T., Ballesta-Illan, E. and Dominguez, M.** (2015). Robust intestinal homeostasis relies on cellular plasticity in enteroblasts mediated by miR-8-Escargot switch. *EMBO J.* **34**, 2025-2041.
**Apidianakis, Y., Pitsouli, C., Perrimon, N. and Rahme, L.** (2009). Synergy between bacterial infection and genetic predisposition in intestinal dysplasia. *Proc. Natl. Acad. Sci. USA* **106**, 20883-20888.
**Badreddine, R. J. and Wang, K. K.** (2010). Barrett esophagus: an update. *Nat. Rev. Gastroenterol. Hepatol.* **7**, 369-378.
**Benjamini, Y., Krieger, A. M. and Yekutieli, D.** (2006). Adaptive linear step-up procedures that control the false discovery rate. *Biometrika* **93**, 491-507.
**Biteau, B., Hochmuth, C. E. and Jasper, H.** (2008). JNK activity in somatic stem cells causes loss of tissue homeostasis in the aging Drosophila gut. *Cell Stem Cell* **3**, 442-455.
**Bodenstein, D.** (1950). The postembryonic development of Drosophila. In *Biology of Drosophila* (ed. M. Demerec), pp. 275-367. New York: Wiley.
**Buchon, N., Broderick, N. A., Chakrabarti, S. and Lemaitre, B.** (2009a). Invasive and indigenous microbiota impact intestinal stem cell activity through multiple pathways in Drosophila. *Genes Dev.* **23**, 2333-2344.
**Buchon, N., Broderick, N. A., Poidevin, M., Pradervand, S. and Lemaitre, B.** (2009b). Drosophila intestinal response to bacterial infection: activation of host defense and stem cell proliferation. *Cell Host Microbe* **5**, 200-211.
**Buchon, N., Osman, D., David, F. P. A., Fang, H. Y., Boquete, J.-P., Deplancke, B. and Lemaitre, B.** (2013). Morphological and molecular characterization of adult midgut compartmentalization in Drosophila. *Cell Rep.* **3**, 1725-1738.
**Chatterjee, M. and Ip, Y. T.** (2009). Pathogenic stimulation of intestinal stem cell response in Drosophila. *J. Cell. Physiol.* **220**, 664-671.
**Chen, J., Xu, N., Huang, H., Cai, T. and Xi, R.** (2016). A feedback amplification loop between stem cells and their progeny promotes tissue regeneration and tumorigenesis. *Elife* **5**, e14330.
**Decotto, E. and Spradling, A. C.** (2005). The Drosophila ovarian and testis stem cell niches: similar somatic stem cells and signals. *Dev. Cell* **9**, 501-510.
**Dutta, D., Dobson, A. J., Houtz, P. L., Gläßer, C., Revah, J., Korzelius, J., Patel, P. H., Edgar, B. A. and Buchon, N.** (2015). Regional cell-specific transcriptome mapping reveals regulatory complexity in the adult Drosophila Midgut. *Cell Rep.* **12**, 346-358.
**Falk, G. W.** (2002). Barrett's esophagus. *Gastroenterology* **122**, 1569-1591.
**Flejou, J.-F.** (2005). Barrett's oesophagus: from metaplasia to dysplasia and cancer. *Gut* **54** Suppl. 1, i6-i12.
**Fox, D. T. and Spradling, A. C.** (2009). The Drosophila hindgut lacks constitutively active adult stem cells but proliferates in response to tissue damage. *Cell Stem Cell* **5**, 290-297.
**Fox, D. T., Morris, L. X., Nystul, T. and Spradling, A. C.** (2009). Lineage analysis of stem cells. In *StemBook [Internet]*. Cambridge (MA): Harvard Stem Cell Institute; 2008-.
**González-Morales, N., Géminard, C., Lebreton, G., Cerezo, D., Coutelis, J.-B. and Noselli, S.** (2015). The atypical cadherin Dachsous controls left-right asymmetry in Drosophila. *Dev. Cell* **33**, 675-689.
**Guo, Z. and Ohlstein, B.** (2015). Stem cell regulation. Bidirectional Notch signaling regulates Drosophila intestinal stem cell multipotency. *Science* **350**, aab0988.
**Harpaz, N. and Polydorides, A. D.** (2010). Colorectal dysplasia in chronic inflammatory bowel disease: pathology, clinical implications, and pathogenesis. *Arch. Pathol. Lab. Med.* **134**, 876-895.
**Heimpel, A. M. and Angus, T. A.** (1960). Bacterial insecticides. *Bacteriol. Rev.* **24**, 266-288.
**Hvid-Jensen, F., Pedersen, L., Drewes, A. M., Sørensen, H. T. and Funch-Jensen, P.** (2011). Incidence of Adenocarcinoma among Patients with Barrett's Esophagus. *New Engl. J. Med.* **365**, 1375-1383.
**Jiang, H., Patel, P. H., Kohlmaier, A., Grenley, M. O., McEwen, D. G. and Edgar, B. A.** (2009). Cytokine/Jak/Stat signaling mediates regeneration and homeostasis in the Drosophila midgut. *Cell* **137**, 1343-1355.
**Losick, V. P., Fox, D. T. and Spradling, A. C.** (2013). Polyploidization and cell fusion contribute to wound healing in the adult Drosophila epithelium. *Curr. Biol.* **23**, 2224-2232.
**Marianes, A. and Spradling, A. C.** (2013). Physiological and stem cell compartmentalization within the Drosophila midgut. *Elife* **2**, e00886.
**Meng, F. W. and Biteau, B.** (2015). A Sox transcription factor is a critical regulator of adult stem cell proliferation in the Drosophila intestine. *Cell Rep.* **13**, 906-914.
**Micchelli, C. A. and Perrimon, N.** (2006). Evidence that stem cells reside in the adult Drosophila midgut epithelium. *Nature* **439**, 475-479.
**Nakagoshi, H.** (2005). Functional specification in the Drosophila endoderm. *Dev. Growth Differ.* **47**, 383-392.
**Nation, J. L.** (2001). *Insect Physiology and Biochemistry*. Boca Rotan: CRC Press.
**O'Brien, L. E., Soliman, S. S., Li, X. and Bilder, D.** (2011). Altered modes of stem cell division drive adaptive intestinal growth. *Cell* **147**, 603-614.
**Ohlstein, B. and Spradling, A.** (2006). The adult Drosophila posterior midgut is maintained by pluripotent stem cells. *Nature* **439**, 470-474.
**Ohlstein, B. and Spradling, A.** (2007). Multipotent Drosophila intestinal stem cells specify daughter cell fates by differential notch signaling. *Science* **315**, 988-992.
**Osman, D., Buchon, N., Chakrabarti, S., Huang, Y.-T., Su, W.-C., Poidevin, M., Tsai, Y.-C. and Lemaitre, B.** (2012). Autocrine and paracrine unpaired signaling regulate intestinal stem cell maintenance and division. *J. Cell Sci.* **125**, 5944-5949.
**Pan, J. and Jin, L. H.** (2014). Rgn gene is required for gut cell homeostasis after ingestion of sodium dodecyl sulfate in Drosophila. *Gene* **549**, 141-148.
**Quante, M., Bhagat, G., Abrams, J. A., Marache, F., Good, P., Lee, M. D., Lee, Y., Friedman, R., Asfaha, S., Dubeykovskaya, Z. et al.** (2012). Bile acid and inflammation activate gastric cardia stem cells in a mouse model of Barrett-like metaplasia. *Cancer Cell* **21**, 36-51.
**Reed, B. H. and Orr-Weaver, T. L.** (1997). The Drosophila gene morula inhibits mitotic functions in the endo cell cycle and the mitotic cell cycle. *Development* **124**, 3543-3553.
**Robertson, C. W.** (1936). The metamorphosis of Drosophila melanogaster, including an accurately timed account of the principal morphological changes. *J. Morphol.* **59**, 351-399.
**San Roman, A. K. and Shivdasani, R. A.** (2011). Boundaries, junctions and transitions in the gastrointestinal tract. *Exp. Cell Res.* **317**, 2711-2718.
**Schneider, C. A., Rasband, W. S. and Eliceiri, K. W.** (2012). NIH Image to ImageJ: 25 years of image analysis. *Nat. Methods* **9**, 671-675.
**Schoenfelder, K. P., Montague, R. A., Paramore, S. V., Lennox, A. L., Mahowald, A. P. and Fox, D. T.** (2014). Indispensable pre-mitotic endocycles promote aneuploidy in the Drosophila rectum. *Development* **141**, 3551-3560.
**Shaheen, N. J. and Richter, J. E.** (2009). Barrett's oesophagus. *Lancet* **373**, 850-861.
**Singer, J. B., Harbecke, R., Kusch, T., Reuter, R. and Lengyel, J. A.** (1996). Drosophila brachyenteron regulates gene activity and morphogenesis in the gut. *Development* **122**, 3707-3718.

**Sotillos, S., Díaz-Meco, M. T., Moscat, J. and Castelli-Gair Hombría, J.** (2008). Polarized subcellular localization of Jak/STAT components is required for efficient signaling. *Curr. Biol.* **18**, 624-629.
**Takashima, S. and Murakami, R.** (2001). Regulation of pattern formation in the Drosophila hindgut by wg, hh, dpp, and en. *Mech. Dev.* **101**, 79-90.
**Takashima, S., Mkrtchyan, M., Younossi-Hartenstein, A., Merriam, J. R. and Hartenstein, V.** (2008). The behaviour of Drosophila adult hindgut stem cells is controlled by Wnt and Hh signalling. *Nature* **454**, 651-655.
**Takashima, S., Paul, M., Aghajanian, P., Younossi-Hartenstein, A. and Hartenstein, V.** (2013). Migration of Drosophila intestinal stem cells across organ boundaries. *Development* **140**, 1903-1911.
**Takashima, S., Aghajanian, P., Younossi-Hartenstein, A. and Hartenstein, V.** (2016). Origin and dynamic lineage characteristics of the developing Drosophila midgut stem cells. *Dev. Biol.* **416**, 347-360.
**Tian, A., Benchabane, H., Wang, Z. and Ahmed, Y.** (2016). Regulation of stem cell proliferation and cell fate specification by Wingless/Wnt signaling gradients enriched at adult intestinal compartment boundaries. *PLoS Genet.* **12**, e1005822.
**Wang, X., Ouyang, H., Yamamoto, Y., Kumar, P. A., Wei, T. S., Dagher, R., Vincent, M., Lu, X., Bellizzi, A. M., Ho, K. Y. et al.** (2011). Residual embryonic cells as precursors of a Barrett's-like metaplasia. *Cell* **145**, 1023-1035.
**Zeng, X. and Hou, S. X.** (2015). Enteroendocrine cells are generated from stem cells through a distinct progenitor in the adult Drosophila posterior midgut. *Development* **142**, 644-653.
**Zhai, Z., Kondo, S., Ha, N., Boquete, J.-P., Brunner, M., Ueda, R. and Lemaitre, B.** (2015). Accumulation of differentiating intestinal stem cell progenies drives tumorigenesis. *Nat. Commun.* **6**, 10219.
**Zorn, A. M. and Wells, J. M.** (2009). Vertebrate endoderm development and organ formation. *Annu. Rev. Cell Dev. Biol.* **25**, 221-251.